International Conference on Mathematics, Computational Methods & Reactor Physics (M&C 2009)
Saratoga Springs, New York, May 3-7, 2009, on CD-ROM, American Nuclear Society, LaGrange Park, IL (2009)

ORDER-CONVERGENCE ANOMALIES IN SECOND-ORDER FINITE ELEMENTS TRANSPORT METHODS

Clif Drumm
Sandia National Laboratories*
Albuquerque, NM 87185-1179
crdrumm@sandia.gov

ABSTRACT

Asymptotic order analysis, i.e. comparing the observed asymptotic order of accuracy with the theoretical value, is a powerful and increasingly-used technique for code verification testing. This technique has proven to be very effective for revealing coding mistakes. In this study, the Method of Manufactured Solutions (MMS) is used to investigate the asymptotic order of accuracy of the second-order algorithms in the SCEPTRE radiation transport code. For the great majority of MMS tests of SCEPTRE, the expected asymptotic order of accuracy is observed. However, for a small number of tests, a lower-than-expected asymptotic order of accuracy is obtained. The anomalously-low order of accuracy is observed in the L_2 and H_1 error norms. However, if a modified H_1 error norm that accounts for the nature of the streaming term in the transport equation is used instead of the L_2 or H_1 error norms, the expected order of accuracy is observed for all of the tests. In these MMS tests, no coding mistakes were found, but it was discovered that a redesign of the MMS test was required, i.e. modifying the error norm being used, in order to obtain agreement between the expected and observed convergence rates.

Key Words: code verification, method of manufactured solutions, finite elements method

1. INTRODUCTION

Code verification is defined by C. J. Roy [1] to be:

> A set of procedures developed to find coding mistakes that affect the numerical discretization.

Several criteria are available for assessing code verification, e.g. error quantification, consistency/convergence, and order of accuracy. Using the Method of Manufactured Solutions (MMS) to test the order of accuracy of the code is the most rigorous and effective approach to code verification [1,2]. In the MMS approach, an analytic solution is specified, which can be simple enough so that the numerical method is expected to provide an "exact" solution (to within roundoff and iterative error) or a more complicated solution to test the grid-convergence behavior of the numerical method. We have used only smooth functions in this study to avoid numerical difficulties caused by discontinuities in the solution, e.g. shadow boundaries.

* Sandia is a multiprogram laboratory operated by Sandia Corporation, a Lockheed Martin Company, for the United States Department of Energy's National Nuclear Security Administration under Contract DEAC04-94AL85000

Once an analytic solution is specified, it is then substituted into the transport equation to obtain the source and boundary conditions corresponding to the specified solution [3]. The numerical algorithm is then run using the specified source and boundary terms, and error norms are computed by comparing the numerical result with the analytic solution. By repeating the calculation for various levels of mesh refinement, the asymptotic order of the error can be obtained and compared with the formal order of accuracy.

SCEPTRE is a massively-parallel finite-elements code, containing several second-order transport algorithms and a first-order sweeps-based algorithm [4,5]. For the great majority of MMS tests of SCEPTRE the expected asymptotic order of accuracy is observed. However, for a small number of tests, a lower-than-expected asymptotic order of accuracy is obtained. The anomalously-low order of accuracy is observed in the L_2 and H_1 error norms. However, if a modified H_1 error norm that accounts for the nature of the streaming term in the transport equation is used instead of the L_2 or H_1 error norms, the expected order of accuracy is observed for all of the tests. In these MMS tests, no coding mistakes were found, but the observed order of convergence did not match that expected a priori. The reason for the discrepancy was not in the MMS test itself but the way in which the results were being assessed [2]. Redesign of the tests to use a more appropriate error norm resulted in agreement between observed and expected convergence rates, showing the value of MMS testing for revealing behavior of the numerical algorithm, in addition to finding coding bugs. The anomalous convergence does not occur for the first-order sweeps-based algorithm.

Table I. Scope of MMS problems considered

Characteristics of the Finite Elements Basis:			
Element Type	triangular/tetrahedral	quadrilateral/hexahedral	
Element Order	linear	quadratic	
Dimensionality	2D	3D	
Characteristics of the Analytic Solution:			
Boundary Condition	non-zero e.g. $e^{-x}e^{-y}$	zero e.g. x(1-x)y(1-y) on unit square	
Expected Accuracy of Discretized Solution	exact e.g. x^2 for quadratic basis	non-exact e.g. $e^{-x}e^{-y}$	
Material Media	purely absorbing	anisotropic scattering	
Characteristic Direction	S_n direction	x, y or z axis	
Error Norm	L_2	H_1 (energy)	H_1 (streaming)

Table I shows the range of MMS problems that have been applied to the SCEPTRE code. Typically, radiation transport problems have non-zero boundary conditions for at least part of the angular range, but we have constructed some MMS tests with zero boundary conditions to

investigate the effect of the boundary terms on the order of accuracy. We have performed both full-transport solutions including scattering and uncollided-flux solutions (purely-absorbing media). The uncollided-flux solutions are easier to analyze, since the full-scattering transport can homogenize and mask directional dependence of the convergence rate. For the uncollided-flux solutions, we investigate characteristic directions that are a part of a fully-symmetric quadrature set and also characteristic directions along the coordinate axes.

2. BACKGROUND

The self-adjoint angular flux (SAAF) equation [6] for purely-absorbing media is described in this section as a model second-order transport algorithm. The nature of the SAAF operator is investigated followed by a description of the various error norms used to obtain the results that are presented in Sec. 3.

2.1. SAAF Equation for the Uncollided Flux

The SAAF equation for purely-absorbing media is

$$-\frac{1}{\sigma_t}\boldsymbol{\Omega}\cdot\nabla\boldsymbol{\Omega}\cdot\nabla\phi(\mathbf{r},\boldsymbol{\Omega})+\sigma_t\phi(\mathbf{r},\boldsymbol{\Omega})=-\frac{1}{\sigma_t}\boldsymbol{\Omega}\cdot\nabla Q(\mathbf{r},\boldsymbol{\Omega})+Q(\mathbf{r},\boldsymbol{\Omega})\ \ for\ \mathbf{r}\in V, \tag{1a}$$

where $\mathbf{r}$ is the spatial position, $\boldsymbol{\Omega}$ is the particle direction of motion, σ_t is the total cross section, $Q(\mathbf{r},\boldsymbol{\Omega})$ is the distributed source and $\phi(\mathbf{r},\boldsymbol{\Omega})$ is the angular fluence. Vacuum boundary conditions are specified for incoming directions with a value of f_b,

$$\phi(\mathbf{r},\boldsymbol{\Omega})=f_b,\ for\ \boldsymbol{\Omega}\cdot\mathbf{n}<0\ \ for\ \mathbf{r}\in\partial V, \tag{1b}$$

and, for outgoing directions, $\boldsymbol{\Omega}\cdot\mathbf{n}>0$, the solution is required to satisfy the first-order transport equation [6]. $\mathbf{n}$ is the unit outward normal. This (and other second-order forms of the transport equation) exhibit the behavior of a degenerate elliptic or parabolic PDE, as is revealed by the determinant of the coefficient matrix of the streaming term. For the direction vector in terms of the direction cosines, $\boldsymbol{\Omega}=(\mu_x,\mu_y,\mu_z)$, the streaming term is

$$\boldsymbol{\Omega}\cdot\nabla\boldsymbol{\Omega}\cdot\nabla\phi(\mathbf{r},\boldsymbol{\Omega})=\left(\mu_x\frac{\partial}{\partial x}+\mu_y\frac{\partial}{\partial y}+\mu_z\frac{\partial}{\partial z}\right)\left(\mu_x\frac{\partial\phi}{\partial x}+\mu_y\frac{\partial\phi}{\partial y}+\mu_z\frac{\partial\phi}{\partial z}\right), \tag{2a}$$

and the determinant of the coefficient matrix is identically zero:

$$\begin{vmatrix}\mu_x^2 & \mu_x\mu_y & \mu_x\mu_z\\ \mu_x\mu_y & \mu_y^2 & \mu_y\mu_z\\ \mu_x\mu_z & \mu_y\mu_z & \mu_z^2\end{vmatrix}\equiv 0. \tag{2b}$$

2.2 Error Norms

The variational formulation of the SAAF equation in purely-absorbing media is [7]

$$F[\phi]=\frac{1}{\sigma_t}\left\langle(\boldsymbol{\Omega}\cdot\nabla\phi)^2\right\rangle+\sigma_t\left\langle\phi^2\right\rangle+\oint_{\boldsymbol{\Omega}\cdot\boldsymbol{n}>0}\int\phi^2|\boldsymbol{\Omega}\cdot\boldsymbol{n}|dsd\boldsymbol{\Omega}-2\langle\phi,Q\rangle-\frac{2}{\sigma_t}\langle\boldsymbol{\Omega}\cdot\nabla\phi,Q\rangle-2\oint_{\boldsymbol{\Omega}\cdot\boldsymbol{n}<0}\int\phi\,f_b|\boldsymbol{\Omega}\cdot\boldsymbol{n}|dsd\boldsymbol{\Omega}, \quad (3)$$

where < > indicates integration over space and angle. Based on the numerical error, $\varepsilon_h(\boldsymbol{r},\boldsymbol{\Omega})$, which is the difference between the analytic solution and the numerical solution,

$$\varepsilon_h(\boldsymbol{r},\boldsymbol{\Omega})=\phi(\boldsymbol{r},\boldsymbol{\Omega})-\phi_h(\boldsymbol{r},\boldsymbol{\Omega}), \quad (4)$$

the L_2 and H_1 norms are given by

$$L_2\ norm\ \left(\iint\left|\varepsilon_h(\boldsymbol{r},\boldsymbol{\Omega})\right|^2 d\boldsymbol{r}\,d\boldsymbol{\Omega}\right)^{1/2} \quad (5)$$

$$H_1\ energy\ norm\ \left(\iint\nabla\varepsilon_h(\boldsymbol{r},\boldsymbol{\Omega})\cdot\nabla\varepsilon_h(\boldsymbol{r},\boldsymbol{\Omega})\,d\boldsymbol{r}\,d\boldsymbol{\Omega}\right)^{1/2}. \quad (6)$$

As noted previously, for most of the SCEPTRE MMS tests, the L_2 and H_1 error norms give the expected convergence behavior. However, for a few tests, less-than-expected convergence is observed. We here define a new error norm, based on the variational formulation, that results in more consistent convergence behavior. Referring the first term in the variational formulation, Eq. (3), it seems reasonable to use the following semi norm as a measure of the error:

$$H_1\ streaming\ norm\left(\iint\left|\boldsymbol{\Omega}\cdot\nabla\varepsilon_h(\boldsymbol{r},\boldsymbol{\Omega})\right|^2 d\boldsymbol{r}\,d\boldsymbol{\Omega}\right)^{1/2}. \quad (7)$$

This error norm is similar to the H_1 energy norm but takes into account the directional dependence of the result. This error norm gives the expected convergence rates for all of the MMS tests considered, even those where the L_2 and H_1 error norms give anomalously-low convergence rates.

3. RESULTS

In this section we present results for MMS transport problems *with scattering*, including a test that exhibits a lower-than-expected convergence rate. The even-odd parity flux (EOPF) second-order form of the transport equation [7] is used for these analyses. We then examine the anomalous test case *without scattering*, to evaluate the spatial convergence properties for individual characteristic directions of motion. Finally, we present results for problems expected to provide exact agreement between numerical and analytic results, to within roundoff and convergence errors.

3.1 EOPF Transport with Scattering

The even-parity form of the transport equation is [7]

$$-\mathbf{\Omega}\cdot\nabla\Re_{-}^{-1}\mathbf{\Omega}\cdot\nabla\phi^{+}(r,\mathbf{\Omega})+\Re_{+}\phi^{+}(r,\mathbf{\Omega})=-\mathbf{\Omega}\cdot\nabla\Re_{-}^{-1}Q^{-}(r,\mathbf{\Omega})+Q^{+}(r,\mathbf{\Omega})\ \text{for}\, r\in V, \tag{8}$$

where the even- and odd-parity removal operators are

$$\Re_{+}\circ=\sigma_{t}\circ-\sum_{l\,\text{even}}\sigma_{s,l}\int P_{l}(\mathbf{\Omega}\cdot\mathbf{\Omega}')\circ d\mathbf{\Omega}' \tag{9a}$$

$$\Re_{-}^{-1}\circ=\frac{1}{\sigma_{t}}\circ+\frac{1}{\sigma_{t}}\sum_{l\,\text{odd}}\frac{\sigma_{s,l}}{\sigma_{t}-\sigma_{s,l}}\int P_{l}(\mathbf{\Omega}\cdot\mathbf{\Omega}')\circ d\mathbf{\Omega}' \tag{9b}$$

where $\boldsymbol{r}$ is the spatial position, $\mathbf{\Omega}$ is the particle direction of motion, σ_t is the total cross section, $\sigma_{s,l}$ are the Legendre moments of the scattering cross section, $Q^{\pm}(\boldsymbol{r},\mathbf{\Omega})$ are the symmetric and anti-symmetric components of the distributed source and $\phi^{+}(\boldsymbol{r},\mathbf{\Omega})$ is the symmetric component of the angular fluence.

The model problem for this series of MMS tests has the following parameters: unit square, unit total cross section, σ_t=1, linearly-anisotropic scattering with scattering ratio of ½:

$$\sigma_{s}(\mu_{0})=\frac{1}{8\pi}(1+\mu_{0}), \tag{10a}$$

which corresponds to scattering moments of

$$\sigma_{s,0}=\tfrac{1}{2},\quad and\quad \sigma_{s,1}=\tfrac{1}{6}. \tag{10b}$$

The unit square is uniformly meshed and refined with quadrilateral elements, and then the quadrilaterals are subdivided to generate a regular triangular mesh, as shown in Figure 1. For two-dimensional symmetry, the solution must be independent of z and symmetric in μ_z, and the manufactured solution chosen for these tests is

$$\phi(\mathbf{r},\mathbf{\Omega})=e^{-x}e^{-y}(1+\mu_{x}+\mu_{y})\mu_{z}^{2}. \tag{11}$$

The even- and odd-parity distributed source terms for this MMS problem are

$$Q^{+}(\mathbf{r},\mathbf{\Omega})=e^{-x}e^{-y}\left[(1+\mu_{x}+\mu_{y})(1-\mu_{x}-\mu_{y})\mu_{z}^{2}-\frac{1}{6}\right], \tag{12a}$$

and

$$Q^{-}(\mathbf{r},\mathbf{\Omega})=-\frac{1}{30}e^{-x}e^{-y}(\mu_{x}+\mu_{y}). \tag{12b}$$

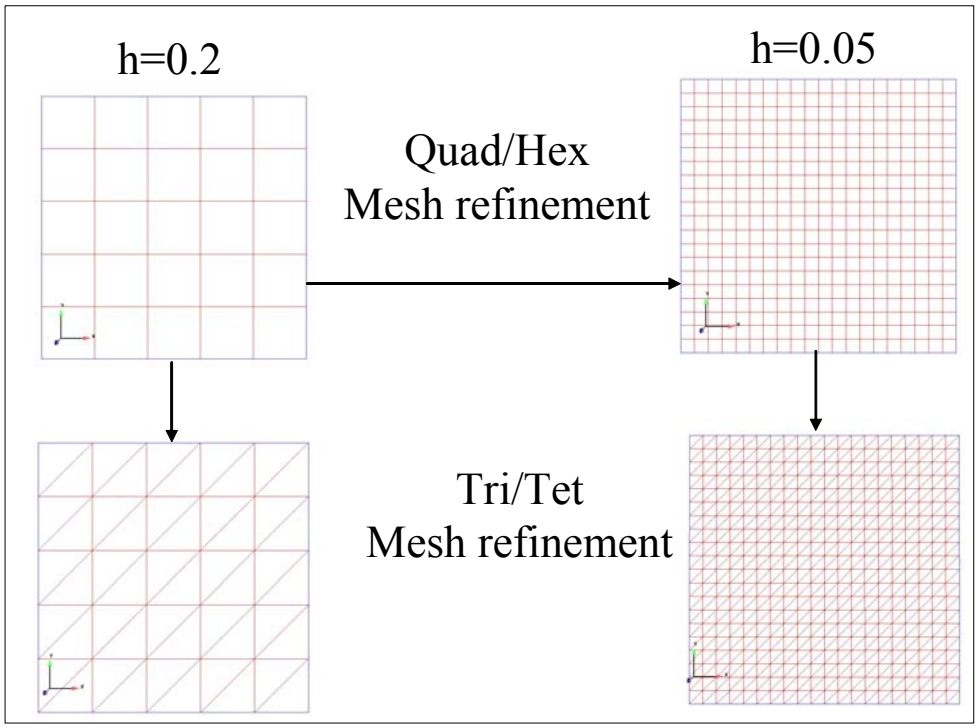

Figure 1. Mesh refinement strategy for various element types.

Tables IIa through IIc show results for linear-quadrilateral, quadratic-quadrilateral and linear triangular meshes, respectively, and the results show smooth convergence to the expected values. In the tables, p is the rate of convergence between each level of mesh refinement. The results shown in Table IId for quadratic-triangular elements, however, show an order less than expected convergence rate for the L_2 and H_1 energy norms, but continue to show expected behavior for the H_1 streaming norm. These results are for the even-parity equation, and results for the odd-parity equation are similar, though not presented here.

Table IIa. Order of accuracy results for MMS model problem with scattering on regular linear quadrilateral (quad4) mesh

	L_2 error norm		H_1 error norm		H_1 streaming error norm	
h	**ε**	**p**	**ε**	**p**	**ε**	**p**
1	$3.12\text{x}10^{-2}$		$8.15\text{x}10^{-2}$		$2.47\text{x}10^{-2}$	
½	$8.42\text{x}10^{-3}$	1.89	$4.05\text{x}10^{-2}$	1.01	$1.38\text{x}10^{-2}$	0.834
¼	$2.18\text{x}10^{-3}$	1.95	$2.02\text{x}10^{-2}$	1.00	$7.20\text{x}10^{-3}$	0.944
⅛	$5.60\text{x}10^{-4}$	1.96	$1.01\text{x}10^{-2}$	1.01	$3.67\text{x}10^{-3}$	0.972
1/16	$1.43\text{x}10^{-4}$	1.97	$5.01\text{x}10^{-3}$	1.01	$1.85\text{x}10^{-3}$	0.987
1/32	$3.63\text{x}10^{-5}$	1.98	$2.49\text{x}10^{-3}$	1.01	$9.30\text{x}10^{-4}$	0.994
expected		2		1		1

Table IIb. Order of accuracy results for MMS model problem with scattering on regular quadratic quadrilateral (quad8) mesh

h	L_2 error norm		H_1 error norm		H_1 streaming error norm	
	ε	p	ε	p	ε	p
1	$1.75\text{x}10^{-3}$		$1.07\text{x}10^{-2}$		$3.59\text{x}10^{-3}$	
½	$2.10\text{x}10^{-4}$	3.06	$2.66\text{x}10^{-3}$	2.01	$9.32\text{x}10^{-4}$	1.95
¼	$2.57\text{x}10^{-5}$	3.03	$6.60\text{x}10^{-4}$	2.01	$2.36\text{x}10^{-4}$	1.98
⅛	$3.18\text{x}10^{-6}$	3.02	$1.63\text{x}10^{-4}$	2.01	$5.96\text{x}10^{-5}$	1.99
1/16	$3.94\text{x}10^{-7}$	3.01	$4.04\text{x}10^{-5}$	2.01	$1.50\ \text{x}10^{-5}$	1.99
1/32	$4.90\text{x}10^{-8}$	3.01	$1.00\text{x}10^{-5}$	2.01	$3.75\text{x}10^{-6}$	2.00
expected		3		2		2

Table IIc. Order of accuracy results for MMS model problem with scattering on regular linear triangular (tri3) mesh

h	L_2 error norm		H_1 error norm		H_1 streaming error norm	
	ε	p	ε	p	ε	p
1	$4.02\text{x}10^{-2}$		$1.24\text{x}10^{-1}$		$4.21\text{x}10^{-2}$	
½	$1.28\text{x}10^{-2}$	1.65	$7.93\text{x}10^{-2}$	0.643	$2.56\text{x}10^{-2}$	0.716
¼	$3.81\text{x}10^{-3}$	1.75	$4.33\text{x}10^{-2}$	0.874	$1.47\text{x}10^{-2}$	0.805
⅛	$1.09\text{x}10^{-3}$	1.81	$2.25\text{x}10^{-2}$	0.942	$7.84\text{x}10^{-3}$	0.901
1/16	$2.99\text{x}10^{-4}$	1.86	$1.13\text{x}10^{-2}$	0.990	$4.06\text{x}10^{-3}$	0.951
1/32	$7.89\text{x}10^{-5}$	1.92	$5.64\text{x}10^{-3}$	1.01	$2.06\text{x}10^{-3}$	0.977
1/64	$2.06\text{x}10^{-5}$	1.94	$2.81\text{x}10^{-3}$	1.01	$1.04\text{x}10^{-3}$	0.990
1/128	$5.39\text{x}10^{-6}$	1.93	$1.40\text{x}10^{-3}$	1.01	$5.20\text{x}10^{-4}$	0.996
1/256	$1.42\text{x}10^{-6}$	1.93	$6.95\text{x}10^{-4}$	1.01	$2.60\text{x}10^{-4}$	0.998
1/512	$3.76\text{x}10^{-7}$	1.91	$3.47\ \text{x}10^{-4}$	1.00	$1.30\text{x}10^{-4}$	0.999
expected		2		1		1

We took a number of steps to eliminate any potential causes of the anomalous behavior: increasing element and edge quadrature integration orders to 9, increasing error norm integration order to 20, using a direct solve rather than an iterative solve to eliminate iterative convergence error, and comparing results for small systems with the Maple analytic solution of the linear system. These steps virtually rule out coding mistakes as a source of the anomalous behavior.

Table IId. Order of accuracy results for MMS model problem with scattering on regular quadratic triangular (tri6) mesh

	L_2 error norm		H_1 error norm		H_1 streaming error norm	
h	ε	p	ε	p	ε	p
1	$3.92\text{x}10^{-3}$		$2.70\text{x}10^{-2}$		$8.55\text{x}10^{-3}$	
½	$5.98\text{x}10^{-4}$	2.71	$8.36\text{x}10^{-3}$	1.69	$2.63\text{x}10^{-3}$	1.70
¼	$8.36\text{x}10^{-5}$	2.84	$2.33\text{x}10^{-3}$	1.84	$7.53\text{x}10^{-4}$	1.81
⅛	$1.10\text{x}10^{-5}$	2.92	$6.19\text{x}10^{-4}$	1.91	$2.02\text{x}10^{-4}$	1.90
1/16	$1.47\text{x}10^{-6}$	2.91	$1.79\text{x}10^{-4}$	1.79	$5.24\text{x}10^{-5}$	1.95
1/32	$2.24\text{x}10^{-7}$	2.72	$6.37\text{x}10^{-5}$	1.49	$1.33\text{x}10^{-5}$	1.98
1/64	$4.27\text{x}10^{-8}$	2.39	$2.77\text{x}10^{-5}$	1.20	$3.36\text{x}10^{-6}$	1.99
1/128	$9.70\text{x}10^{-9}$	2.14	$1.33\text{x}10^{-5}$	1.06	$8.43\text{x}10^{-7}$	1.99
1/256	$2.36\text{x}10^{-9}$	2.04	$6.59\text{x}10^{-6}$	1.01	$2.11\text{x}10^{-7}$	2.00
expected		3		2		2

3.2 SAAF Transport Without Scattering

The results presented in the previous section are for transport with scattering, so that all of the directions are coupled together. In order to investigate the convergence behavior for individual characteristic directions, in this section we model an MMS problem similar to that studied in the previous section but without scattering, so that the individual directions are decoupled from each other. The lower-than-expected convergence rates occur for problems where the characteristic direction of radiation transport is along mesh boundaries.

The MMS solution considered in this section is the same as before,

$$\phi(\mathbf{r},\boldsymbol{\Omega}) = e^{-x}e^{-y}\left(1+\mu_x+\mu_y\right)\mu_z^2 \tag{12}$$

and the distributed source term is

$$Q(\mathbf{r},\boldsymbol{\Omega}) = e^{-x}e^{-y}\left(1+\mu_x+\mu_y\right)\left(1-\mu_x-\mu_y\right)\mu_z^2. \tag{13}$$

Table IIIa shows the convergence results for the three different error norms for $\Omega = \left(1/\sqrt{3}, 1/\sqrt{3}, 1/\sqrt{3}\right)$, showing the less-than-expected convergence orders for the L_2 and H_1 error norms. The convergence rates of the L_2 and H_1 error norms are converging to one order less than the theoretical result, as compared to what would be expected for an elliptic PDE. The H_1 streaming error norm, however, converges smoothly to the expected value.

Table IIIb shows convergence results for a different characteristic direction, **Ω**=(0.3500,0.8689,0.3500), which is one of the directions in an S_4 fully-symmetric quadrature set. For this MMS test, all three error norms smoothly converge to the expected values. We have found that for many cases, the convergence of the L_2 and H_1 error norms is degraded for

directions along element boundaries in the mesh. It appears that the error propagates for characteristic directions along element boundaries, while the error is damped otherwise. The H_1 streaming error norm, however, is not sensitive to the alignment of the radiation direction and element boundaries. Though not included here, we have also performed convergence analyses for characteristic directions along the coordinate axes, which also are along element boundaries in the mesh, and observe the lower-than-expected convergence rates for the L_2 and H_1 error norms, but not for the H_1 streaming error norm.

Table IIIc shows convergence results for an irregular mesh, which prevents streaming along element boundaries, for $\Omega = \left(1/\sqrt{3}, 1/\sqrt{3}, 1/\sqrt{3}\right)$. The convergence behavior is less smooth than the previous results due to the somewhat random nature of the mesh refinement, but the observed convergence orders for all three error norms are better than expected.

Table IIIa. Order analysis results for $\Omega = \left(1/\sqrt{3}, 1/\sqrt{3}, 1/\sqrt{3}\right)$ on regular quadratic triangular (tri6) Mesh

	L_2 error norm		H_1 error norm		H_1 streaming error norm	
h	**ε**	**p**	**ε**	**p**	**ε**	**p**
1	$8.43\text{x}10^{-3}$		$6.63\text{x}10^{-2}$		$3.95\text{x}10^{-2}$	
1/2	$1.19\text{x}10^{-3}$	2.82	$1.87\text{x}10^{-2}$	1.83	$1.06\text{x}10^{-2}$	1.90
1/4	$1.66\text{x}10^{-4}$	2.85	$5.55\text{x}10^{-3}$	1.75	$2.69\text{x}10^{-3}$	1.97
1/8	$2.67\text{x}10^{-5}$	2.64	$2.02\text{x}10^{-3}$	1.46	$6.75\text{x}10^{-4}$	1.99
1/16	$5.36\text{x}10^{-6}$	2.32	$8.91\text{x}10^{-4}$	1.18	$1.69\text{x}10^{-4}$	2.00
1/32	$1.25\text{x}10^{-6}$	2.11	$4.29\text{x}10^{-4}$	1.05	$4.22\text{x}10^{-5}$	2.00
1/64	$3.04\text{x}10^{-7}$	2.03	$2.13\text{x}10^{-4}$	1.01	$1.06\text{x}10^{-5}$	2.00
expected		3		2		2

Table IIIb. Order analysis results for Ω=(0.3500,0.8689,0.3500) on regular quadratic triangular (tri6) mesh

	L_2 error norm		H_1 error norm		H_1 streaming error norm	
h	**ε**	**p**	**ε**	**p**	**ε**	**p**
1	$7.77\text{x}10^{-3}$		$6.08\text{x}10^{-2}$		$4.25\text{x}10^{-2}$	
1/2	$1.32\text{x}10^{-3}$	2.56	$1.97\text{x}10^{-2}$	1.62	$1.18\text{x}10^{-2}$	1.85
1/4	$1.70\text{x}10^{-4}$	2.95	$5.05\text{x}10^{-3}$	1.97	$3.09\text{x}10^{-3}$	1.93
1/8	$2.14\text{x}10^{-5}$	2.99	$1.28\text{x}10^{-3}$	1.98	$7.88\text{x}10^{-4}$	1.97
1/16	$2.69\text{x}10^{-6}$	2.99	$3.20\text{x}10^{-4}$	1.99	$1.99\text{x}10^{-4}$	1.96
1/32	$3.36\text{x}10^{-7}$	3.00	$8.01\text{x}10^{-5}$	2.00	$5.00\text{x}10^{-5}$	1.99
expected		3		2		2

Table IIIc. Order analysis results for $\Omega = \left(1/\sqrt{3}, 1/\sqrt{3}, 1/\sqrt{3}\right)$ on irregular quadratic triangular (tri6) mesh

h	L_2 error norm		H_1 error norm		H_1 streaming error norm	
	ε	p	ε	p	ε	p
1	$8.43\text{x}10^{-3}$		$6.63\text{x}10^{-2}$		$3.95\text{x}10^{-2}$	
½	$1.63\text{x}10^{-3}$	2.37	$1.84\text{x}10^{-2}$	1.85	$1.10\text{x}10^{-2}$	1.85
¼	$1.48\text{x}10^{-4}$	3.46	$3.91\text{x}10^{-3}$	2.24	$2.02\text{x}10^{-3}$	2.45
⅛	$1.45\text{x}10^{-5}$	3.35	$7.27\text{x}10^{-4}$	2.43	$4.34\text{x}10^{-4}$	2.22
1/16	$1.64\text{x}10^{-6}$	3.15	$1.62\text{x}10^{-4}$	2.16	$1.05\text{x}10^{-4}$	2.05
1/32	$1.73\text{x}10^{-7}$	3.24	$3.64\text{x}10^{-5}$	2.16	$2.40\text{x}10^{-5}$	2.13
expected		3		2		2

In order to further illustrate the effect of the characteristic direction on the error, Figs. 2a and 2b show the spatial dependence of the absolute error for $\Omega = \left(1/\sqrt{3}, 1/\sqrt{3}, 1/\sqrt{3}\right)$ and $\Omega = (0.3500, 0.8689, 0.3500)$, respectively, showing the dramatic reduction in the error for the direction not along element boundaries. Fig. 2c shows the spatial dependence of the error for the irregular mesh, corresponding to the results shown in Table IIIc.

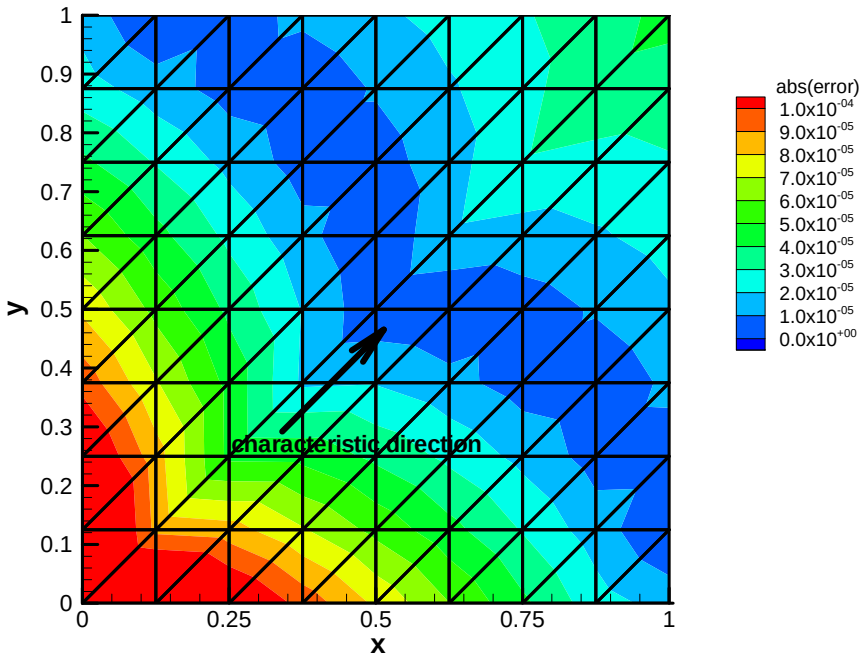

Figure 2a. Absolute error for $\Omega = \left(1/\sqrt{3}, 1/\sqrt{3}, 1/\sqrt{3}\right)$ on regular triangular mesh.

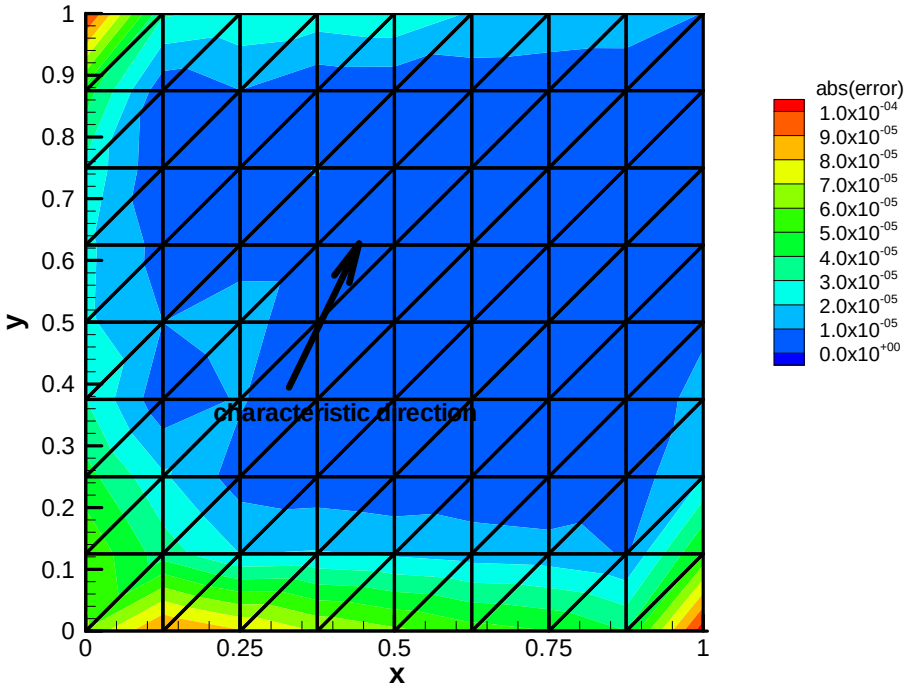

Figure 2b. Absolute error for $\Omega = (0.3500, 0.8689, 0.3500)$ on regular triangular mesh.

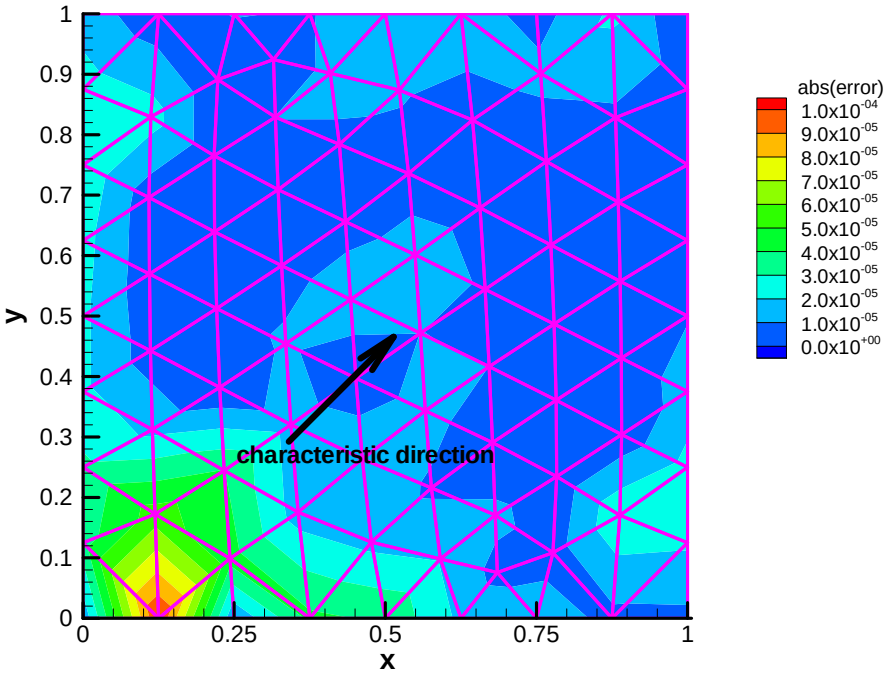

Figure 2c. Absolute error for $\Omega = (1/\sqrt{3}, 1/\sqrt{3}, 1/\sqrt{3})$ on irregular triangular mesh.

3.3 First-Order Results

The anomalous convergence behavior does not occur for the first-order sweeps-base solver in SCEPTRE. Table IV shows the convergence results for the first-order solver, showing expected convergence behavior for all three error norms. Fig. 3. shows the spatial distribution of the absolute error. The first-order solver is based on discontinuous finite-elements basis functions, as opposed to the second-order algorithms, which are based on continuous finite-element basis functions, as is evident in the figures. All of the first-order MMS test problems done to date have shown the expected order of convergence.

3.4 Problems Expected to Yield Exact Solutions to Within Round Off and Convergence Error

Table V lists the error norm results for MMS problems with low-order polynomial analytic solutions, which should be handled exactly in space and angle. The two-dimensional solutions are independent of z and symmetric in μ_z, and the spatial dependence of the solutions is chosen to be as high as the order of the set of finite-elements basis functions that are being tested.

Iterative convergence error is defined such that the relative 2-norm of the residual is less than a prescribed value (10^{-12} for the results presented here),

$$\frac{\|\boldsymbol{r}\|_2}{\|\boldsymbol{r}_0\|_2} < 10^{-12}. \tag{14}$$

In all cases, the observed error norms are less than 10^{-10}. The error norms listed in Table V are computed from integrals over the entire spatial domain, rather than just at the nodes, while the convergence criterion, Eq. (14), is nodal metric, so the error norms are not guaranteed to be less than the convergence error defined this way.

4. SUMMARY

This article presents a small subset of the MMS tests that have been performed as a part of the verification of the SCEPTRE radiation transport code. In addition to providing code verification, the following conclusions can be drawn from these analyses: 1) use of a modified H_1 semi norm that is based on the underlying variational principle and includes the characteristic directions of the radiation transport provides more consistent convergence results, 2) avoiding characteristic directions that lie along boundaries in the FEM mesh results in more predictable convergence results, and 3) the anomalous behavior is not seen when using the first-order sweeps-based solver. In this study, no new coding mistakes were found, but the MMS testing revealed behavior of the numerical algorithm under various situations and resulted in better defined MMS tests by pointing to a more appropriate error norm to be used for assessing the results.

Table IV. Order analysis results for $\Omega = \left(1/\sqrt{3}, 1/\sqrt{3}, 1/\sqrt{3}\right)$ on regular quadratic triangular (tri6) mesh: first order results

h	L_2 error norm		H_1 error norm		H_1 streaming error norm	
	ε	p	ε	p	ε	p
1	$6.64\text{x}10^{-3}$		$7.13\text{x}10^{-2}$		$4.84\text{x}10^{-2}$	
1/2	$9.69\text{x}10^{-4}$	2.78	$2.01\text{x}10^{-2}$	1.83	$1.36\text{x}10^{-2}$	1.83
1/4	$1.28\text{x}10^{-4}$	2.92	$5.22\text{x}10^{-3}$	1.94	$3.54\text{x}10^{-3}$	1.94
1/8	$1.65\text{x}10^{-5}$	2.96	$1.33\text{x}10^{-3}$	1.98	$9.01\text{x}10^{-4}$	1.98
1/16	$2.08\text{x}10^{-6}$	2.98	$3.35\text{x}10^{-4}$	1.99	$2.27\text{x}10^{-4}$	1.99
1/32	$2.61\text{x}10^{-7}$	2.99	$8.40\text{x}10^{-5}$	2.00	$5.69\text{x}10^{-5}$	2.00
expected		3		2		2

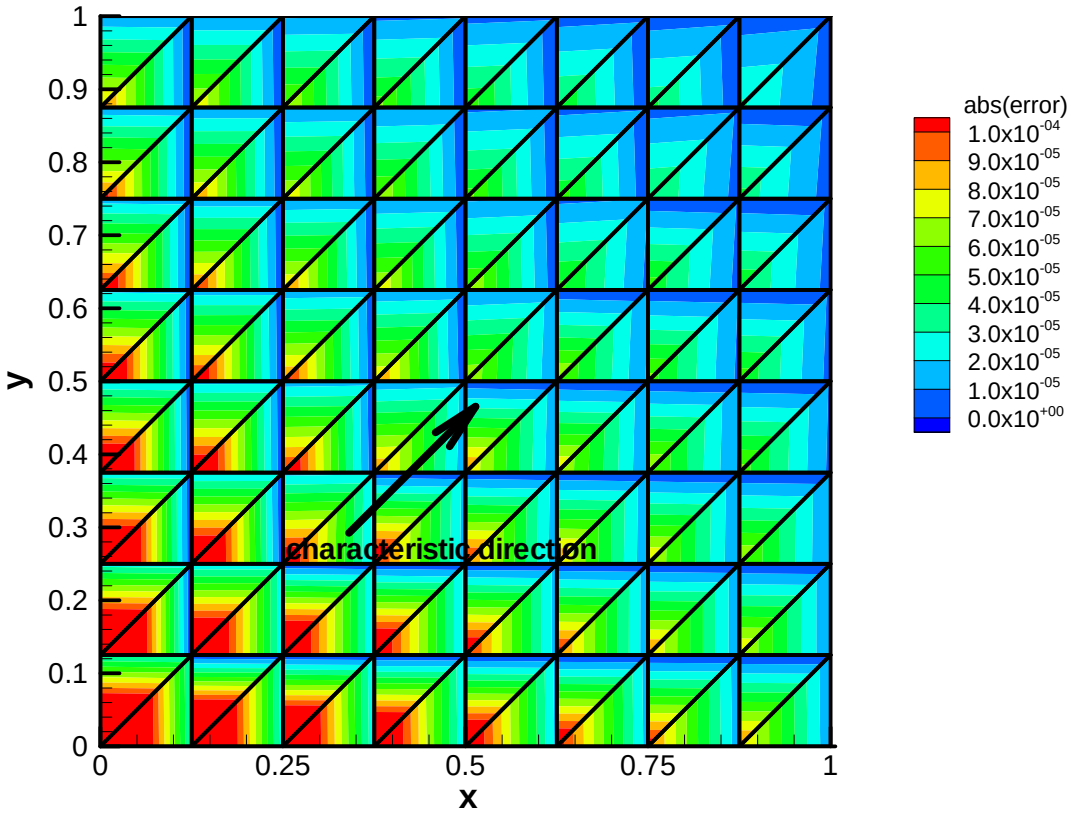

Figure 3. Absolute error for $\Omega = \left(1/\sqrt{3}, 1/\sqrt{3}, 1/\sqrt{3}\right)$ on regular triangular mesh computed with first-order transport solver.

Table V. Results of MMS tests including linearly-anisotropic scattering, expected to be "exact" to within round-off and iterative error

element type	Analytic Solution	h	S_n order	L_2 norm	H_1 energy norm	H_1 streaming norm
tri3	$(1+x+y)(1+\mu_x+\mu_y+\mu_z^2)$	1/8	8	3.84×10^{-14}	4.14×10^{-13}	1.00×10^{-13}
tri6	$(1+x+y)^2\ (1+\mu_x+\mu_y+\mu_z^2)$	"	"	8.05×10^{-13}	1.11×10^{-11}	1.22×10^{-12}
quad4	$(1+x)(1+y)\ (1+\mu_x+\mu_y+\mu_z^2)$	"	"	4.69×10^{-14}	3.25×10^{-13}	1.04×10^{-13}
quad8	$(1+x)(1+y)(1+x+y)(1+\mu_x+\mu_y+\mu_z^2)$	"	"	1.05×10^{-13}	1.40×10^{-12}	2.30×10^{-13}
tet4	$(1+x+y+z)\ (1+\mu_x+\mu_y+\mu_z)$	1/4	4	7.24×10^{-13}	5.20×10^{-12}	1.30×10^{-12}
tet10	$(1+x+y+z)^2\ (1+\mu_x+\mu_y+\mu_z)$	"	"	3.25×10^{-12}	9.12×10^{-11}	5.54×10^{-12}
hex8	$(1+x)(1+y)(1+z)\ (1+\mu_x+\mu_y+\mu_z)$	"	"	7.61×10^{-13}	6.92×10^{-12}	2.17×10^{-12}
hex20	$(1+x)(1+y)(1+z)(1+x+y+z)(1+\mu_x+\mu_y+\mu_z)$	"	"	4.48×10^{-12}	3.68×10^{-11}	9.65×10^{-12}

ACKNOWLEDGMENTS

Appreciation is expressed to Patrick Knupp, Shawn Pautz, Brian Carnes and Kevin Copps at Sandia National Laboratories for useful discussions and insights.

REFERENCES

1. C. J. Roy, "Review of code and solution verification procedures for computational simulation," *J. Comp. Phys.,* **205**, pp. 131-156 (2005).
2. P. Knupp and K. Salari, *Verification of Computer Codes in Computational Science and Engineering*, Chapman & Hall/CRC, Boca Raton, USA (2003).
3. W. R. Martin and J. J. Duderstadt, "Finite Element Solutions of the Neutron Transport Equation with Application to Strong Heterogeneities," *Nucl. Sci. Eng.,* **62**, pp. 371-390 (1977).
4. C.R. Drumm, et al., "Coupled Electron-Photon Transport with the CEPTRE Code," *Mathematics and Computation, Supercomputing, Reactor Physics and Nuclear and Biological Applications*, Avignon, France, Sept. 12-15, 2005.
5. S. D. Pautz, et al., " Parallel Discrete Ordinates Methods in the SCEPTRE Project," *2009 International Conference on Mathematics, Computational Methods & Reactor Physics (M&C 2009)*, Saratoga Springs, NY, May 3-7, 2009.
6. J. E. Morel and J. M. McGhee, "A Self-Adjoint Angular Flux Equation," *Nucl. Sci. Eng.,* **132**, pp. 312-325 (1999).
7. J. J. Duderstadt and W. R. Martin, *Transport Theory*, Wiley-Interscience, New York, USA (1979).